Evolved Gas Analysis–Mass Spectrometry Exposes Polymer Network Structures

Derek B. Dwyer, Nidia C. Gallego, Jisue Braatz, Joshua T. Damron, Logan T. Kearney, J. L. Niedziela, Andrew Miskowiec*

Oak Ridge National Laboratory, P.O. Box 2008 MS-6117, Oak Ridge, TN, USA

*Corresponding author: dwyerdb@ornl.gov

Keywords: product-specific kinetics, polymer network structure, evolved gas analysis, mass spectrometry, pyrolysis, packing density

Abstract: Polymer network structures in epoxy thermosets play an important role in the final thermoset material properties. However, analytical characterization of these network structures is difficult due to their amorphous nature. In this work, the application of evolved gas analysis–mass spectrometry (EGA-MS) to characterize the polymer network structures of bisphenol A (BPA)-based thermosets is demonstrated. Analytical characterization of the polymer network structures is accomplished by monitoring the Product Specific Kinetics (PSK) of BPA monomer formation during thermal degradation investigations. We relate observed differences in the activation energy (E_a) of BPA monomer formation to the local packing environment around the BPA monomer units within the polymer network. Variations in the local environment related to the polymer networks

manifest qualitatively as broadening in the thermal profile of the BPA monomer evolution and quantitatively as changes in the activation energy (E_a). Three BPA thermoset formulations were investigated; two amine cured thermoset with 4,4'-diaminodiphenylmethane (DDM) or poly (propylene glycol) bis(2-amino-propyl ether) (PPG400) and a homopolymerized thermoset via curing with Epikure 3253 catalyst (3253). Results revealed the 3253 thermoset contained two distinct packing densities in the polymer network while DDM and PPG400 thermosets had uniform distributions of packing densities. Results from the DDM thermoset revealed a gradually decreasing E_a while the apparent E_a of PPG400 was consistent over the entire degradation. These differences in E_a were concluded to stem from the flexibility of the corresponding polymer networks and ability of the network components to rearrange and occupy formed voids. Due the minimal sample required for analysis (100-200 μg) this EGA-MS technique has great potential for post-production evaluation of composite parts to identify changes in the polymer networks from use and aging which could signal compromised performance.

Introduction

Epoxy thermosets are a versatile class of polymer materials used in many applied and industrial settings.[1] Although amorphous, the structural arrangement, density, and isomeric balance of thermoset polymer networks has been demonstrated to affect final thermoset material properties.[2, 3] Consequently, understanding the packing arrangements of polymer networks is important for predicting final thermoset material properties and to identify changes in the thermoset that could compromise performance in applications. X-ray scattering techniques are commonly employed for characterization of crystalline or semicrystalline polymer networks. However, direct structural elucidation of thermosetting polymer networks with x-ray scattering techniques is inherently difficult because of their amorphous nature.[4-7] Therefore, alternative methods to characterize

networks within amorphous thermosets are needed to inform on the impact of network structures to final material properties.

Recently, evolved gas analysis–mass spectrometry (EGA-MS) has shown potential for interrogating thermally aged polymer networks.[8, 9] One study on bisphenol A diglycidyl ether (BADGE) epoxy thermoset used the major ion of BPA monomer (*m/z* = 213) to gain structural insight into the aged network via BPA monomer formation.[8] At longer age times, two peaks manifested. A low-temperature peak was concluded to stem from dangling chain BPA monomers in the network. Broadening of the primary pyrolysis peak was also observed, and hypothesized to result from cracked chains in the polymer network.[8]

Broadening of the primary pyrolysis peak is understandable because mass spectra collected in scanning mode monitors many ions that comprise the final thermograph. Thermal aging will induce cracked chains and yield a larger distribution of evolved products with different evolution temperatures resulting in the broadening of the pyrolysis peak. However, peak broadening in selected ion monitoring (SIM) mode where only the *m/z* 213 ion is monitored is not as intuitive. Assuming BPA monomer forms via one mechanism, which is the consensuses in the literature,[8, 10-13] and that the *m/z* 213 ion is unique to BPA, then we hypothesize that broadening of the *m/z* 213 pyrolysis peak indicates changes in the local environment of the BPA monomer units. This heterogeneity would stem from changes in local packing densities that would manifest quantitatively as changes in the activation energy of BPA monomer formation between different packing arrangements.

Here, we propose that EGA-MS can be used to interrogate polymer network packing arrangements. We investigated three distinct thermoset formulations using different structural hardeners to induce differences in local BPA monomer packing arrangements. We show that these

packing differences manifest qualitatively as broadened Single Ion Thermograph (SIT) peaks between different thermoset formulations and quantitatively as changes in the kinetics of monomer formation during pyrolysis using recently developed product-specific kinetic (PSK) methodology.[14, 15]

Methods and Materials

Materials

Bisphenol A diglycidyl ether (BADGE), poly (propylene glycol) bis(2-amino-propyl ether) [Mn 400] (PPG400), and 4,4'-Diaminodiphenylmethane (DDM) were purchased from Sigma-Aldrich. Epikure 3253 [2,4,6-Tris(dimethylaminomethyl) phenol] (3253) was received from Miller-Stephenson Chemical Co. Inc. Ideal chemical structures of the BADGE epoxy; DDM and PPG400 hardeners; and 3253 catalyst are shown in **Figure 1**. All chemicals were used as received.

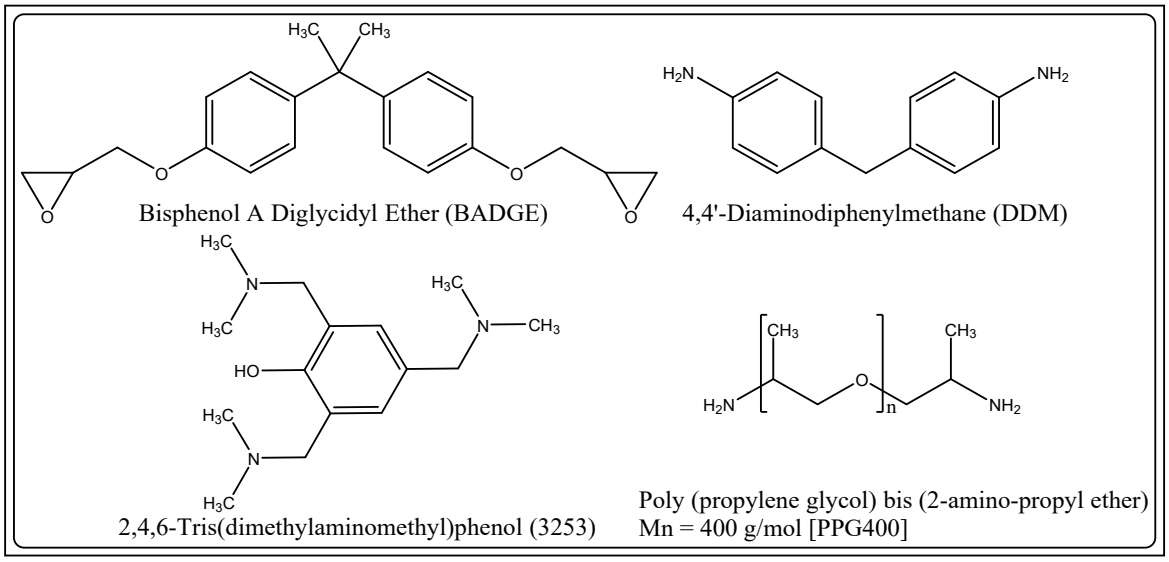

Figure 1. Ideal chemical structures of BADGE epoxy; DDM and PPG400 hardeners; and 3253 catalyst.

Thermoset Synthesis

Amine-cured thermoset BADGE/PPG400 (PPG400) was prepared by mixing epoxy resin and amine hardener at stochiometric ratios of 1:2 so that the number of epoxy functional groups to amine protons is 1:1. PPG400 was cured for 18–20 hrs at 358 K and then post cured at 423 K for 2 hrs. BADGE/DDM (DDM) thermoset was prepared by mixing BADGE epoxy resin with solid DDM pellets at the above mentioned stochiometric ratios. The mixture was then heated at 373 K for 30 min or until DDM hardener completely dissolved in the BADGE epoxy resin. The sample was mixed and cured at 373 K for 3 hrs. DDM thermoset was post cured at 423 K for 2 hrs. Finally, BADGE/3253 (3253) thermoset was prepared by mixing 1.021 g of epoxy resin with 75 μL of 3253 catalyst. The mixture was cured at 358 K for 18–20 hrs then post cured at 423 K for 2 hrs. Cure parameters and sample assignments are shown in Table 1.

Table 1. List of hardeners with initial and post cure temperatures and times with sample assignments.

Hardener	Initial Cure Temp./Time	Post Cure Temp./Time	Sample
3253	358 K, 18-20 hrs	N/A	3253 RT
3253	358 K, 18-20 hrs	423 K, 2hrs	3253 PC
DDM	373 K, 3hrs	N/A	DDM RT
DDM	373 K, 3hrs	423 K, 2hrs	DDM PC
PPG400	358K, 18-20 hrs	N/A	PPG400 RT
PPG400	358K, 18-20 hrs	423K, 2hrs	PPG400 PC

Differential Scanning Calorimetry

Differential Scanning Calorimetry (DSC) was performed on a Discovery DSC250 from TA Instruments. All DSC measurements were performed under nitrogen. Samples were heated at a 5 K/min heating rate from 305 K to 498 K then cooled back down to 305 K prior to a second heating cycle to 498 K. Cure extent was calculated using equation 1.[16]

$$Cure\ \% = \left(1 - \frac{\Delta H_{RC}}{\Delta H_{FC}}\right) * 100 \quad (1)$$

Where ΔH_{RC} is the heat released during the Residual Cure (RC) of a thermoset that has already undergone curing and ΔH_{FC} is the heat released during the Full Cure (FC) of a thermoset that has undergone no curing prior to analysis.

Scanning Electron Microscopy

Scanning Electron Microscopy (SEM) images were taken with a ZEISS Gemini 460 field emission SEM. Powdered samples were put on a Gun Shot Residue (GSR) tab and carbon coated for 5 seconds prior SEM imaging. Images were taken at an accelerating voltage of 1 kV.

Pyrolysis–Gas Chromatography–Mass Spectrometry

Pyrolysis–gas chromatography–mass spectrometry (Py-GC-MS) was performed to confirm *m/z* 213 is a unique ion for a BPA monomer product. Samples were prepared in 80 µL Eco-Cups™ as a powder using a polymer preparation grinding tool (Frontier Laboratories Ltd.) at masses between 100 and 200 µg. Prepared samples were then mounted in a microfurnace (PY-3030D, Frontier Analytical Ltd.) interfaced with an Agilent GC (7890B)-MSD (5977A) with a carrier gas selector (CGS-1050Ex) and selective sampler (SS-1010E) from Frontier Analytical Ltd. An Ultra ALLOY capillary column (UA5-30M-0.25F) 30 m in length, 0.25 mm inner diameter, with a 0.25 µm film was used for product separation. Samples were dropped into the furnace at 873 K for 2 min. The resulting products were carried into the inlet by helium carrier gas at a total flow rate of 64.2 mL/min. Products were split in the inlet at a split ratio of 50:1 with an inlet temperature set at 553 K, a pressure of 63.1 kPa, and purge flow rate of 3 mL/min, resulting in a total flow rate of 60 mL/min with 1.2 mL/min of flow being injected into the GC column. A Microjet cryotrap from Frontier was used to concentrate products at the head of the column before analysis. After the 2 min pyrolysis, the cryotrap was switched off, and the GC oven was heated at the following

parameters: 2 min hold at 313 K then ramped to 593 K at a heating rate of 293 K/min. The MSD scanning range was set to *m/z* 29–500. Detected products were identified using F-search software (version 3.5.2, Frontier Laboratories Ltd.).

Evolved Gas Analysis–Mass Spectrometry

For EGA-MS experiments, the Ultra ALLOY capillary column in the GC oven was replaced with an Ultra ALLOY EGA tube (UADTM-2.5N) measuring 2.5 m in length with an inner diameter of 0.15 mm and an outer diameter of 0.47 mm. Samples were dropped into the microfurnace at 353 K and held for 1 min before heating at 2, 5, or 10 K/min up to 973 K. Products produced during heating are immediately transferred to the inlet held at 553 K by the carrier gas at a total flow of 139.4 mL/min and pressure of 171.8 kPa. The septum purge flow was set at 3 mL/min, resulting in a split flow of 135.2 mL/min with 1.2 mL/min of the flow being injected into the EGA tube. The GC oven was held at a constant 593 K during the experiment to allow for immediate detection of the ions in the mass spectrometer (MS). The MS was run in either scanning mode, *m/z* 29 - 500, for total ion thermographs (TITs) or selected ion monitoring mode monitoring the *m/z* 213 ion for SIT.

Note, some of the thermographs had measurable signal before the pyrolysis peak and an elevated signal at the tail of the peak. This was concluded to be due to cross contamination between experiments. Figure S1 shows the TIT of 3253 at 10 K/min after several rounds of column cleaning before analysis and subsequent post cleaning runs, with no sample, showing the signal carryover after a sample is run. However, the elevated baseline after the pyrolysis peak is not solely carryover but is suspected to result from the char formed in the Eco-Cup from polymer degradation. Because the focus of this work is the primary pyrolysis peak, corrections were performed to remove additional signals from cross contamination and char. An End Points Weighted correction in the

Origin Pro 2022 software was used to correct for these signals. The End Points Weighted correction values for each TIT and SIT are shown in Table S1.

Product-Specific Kinetic Analysis

A detailed discussion of PSK analysis and furnace calibrations can be found in previous publications.[14, 15] In short, PSK is a methodology that uses unique ions of specific products identified via extracted ion chromatography (EIC). Thermographs of the unique ions are obtained via SIM mode or extracted ions from TITs, in this work SIM mode was used to obtain SITs for PSK analysis of the *m*/*z* 213 ion. Isoconversional kinetic methods are then applied to ion thermographs to determine PSKs.

Two trials were performed at three different heating rates (2, 5, and 10 K/min) in SIM mode. Conversion plots were generated from the resulting thermographs using eq 2.

$$\alpha = \frac{AMI_T}{AMI_f} \tag{2}$$

where AMI_T is the accumulated mass intensity at a given temperature, T, AMI_f is the accumulated mass intensity at the final temperature, and α is the extent of conversion.[17] A modification of the Kissinger–Akahira–Sunose equation, eq 3, was used to calculate the apparent activation energy (E_a) from the conversion plots.[18, 19 20]

$$\ln\frac{\beta_i}{T_{\alpha,i}^{1.92}} = Const - 1.0008 \times \frac{E_a}{RT_{\alpha,i}} \tag{3}$$

where β_i is the heating rate, $T_{\alpha,i}$ is the temperature at a specific α and heating rate, and R is the universal gas constant. The activation energy was then calculated from the slope of $\ln(\beta_i/T^{1.92}_{\alpha,i})$ against $1/T_{\alpha,i}$. Associated error bars were calculated using the least squares method from the error in the plotted slopes.

Wide-Angle X-ray Scattering

Measurements of the thermosets were made using a Xeuss 3.0 (Xenocs, France) wide-angle x-ray scattering (WAXS) instrument equipped with a D2+ MetalJet x-ray source (Ga Kα, 9.2 keV,

λ = 1.3414 Å). Quartz capillaries (2 mm thick) were filled with the prepolymer resin and cured. Samples were arranged perpendicular to the beam at sample-to-detector distances of 47 and 900 mm for wide- and small-angle scattering measurements, respectively. 2D images of the scattering patterns were collected on an Eiger 2R 4M hybrid photon counting detector with a pixel dimension of 75 μm^2 (Dectris, Switzerland). The 2D WAXS images were background corrected and reduced in the form of intensity versus scattering vector (Q). The Q range investigated in this work was 0–3.5 Å^{-1}.

Nuclear Magnetic Resonance

Powdered samples were poured into 10 mm glass NMR tubes and measured using direct detection (DD) and Magic Sandwich Echo (MSE) pulse sequences using 90° pulses of 3.5 μs and a spectrometer dead time of 10 μs using a Bruker MQ20 benchtop spectrometer. The data were fit using a co-fit strategy with the MSE and DD free induction decays (FIDs) to extract phase fraction ratios.[21, 22] The MSE provides more of the FID by overcoming dead time issues, giving better shape parameter estimation.[21, 22] However, some relaxation can occur for the rigid component on the timescale of the MSE refocusing block, making the phase weighting of the components from the DD sequence more reliable. Here, we used a three-component phase fit including the Abragam function and two exponentials (eq 4).[23, 24]

$$FID(t) = A_a e^{-0.5(t/T2_a)^2} sin(bt)/(bt) + A_g e^{-(t/T2_g)^{\beta}} + A_{wb} e^{-(t/T2_{wb})^{\alpha}} \quad (4)$$

Fractions were determined by normalizing to the total ($A_a + A_g + A_{wb}$). For fit stability, we fixed $\beta = 2.0$ and $\alpha = 1.5$ with the guidance taken from for rigid crystalline, amorphous rigid, and immobilized phase fractions.[22] Relaxation parameters were similar for each sample and phase fraction with T_{2a} values ranging between 5.6-7 μs, T_{2g} between 16-18 μs, and T_{2wb} 0.75-1.2 ms, providing a clean phase fraction comparison below. The T_2 values for A_a and A_g are

typical for highly rigid polymeric systems while the A_{wb} suggests a softer phase of dangling bonds within the system.[21, 22, 25, 26]

Results and Discussion

Prior to kinetics analysis of these thermosets' evaluation of the extent cure and particle morphology is needed to ensure that the observed kinetics are from BPA monomer formation alone and not artifacts from sample preparation. Preliminary polymer network characterization was performed to provide additional insight into the polymer networks studied. Differential scanning calorimetry was performed on all thermosets and the uncured resin formulations to determine the effective cure of the thermosets from the chosen curing time and temperature, Figure 2 and S1. Two heating cycles were performed to differentiate irreversible transitions, curing, from reversable transitions, glass transition temperature (T_g). The DSC analysis of the uncured resin formulations revealed both DDM and PPG400 thermosets have a single cure peak at approximately 420 K and 400 K respectively, Figure S2. Glass transitions temperatures were identified from the second heating cycles of the uncured resins at ~ 450 K for DDM and ~ 317 K for PPG400, Figure S2. The DSC profile of the uncured 3253 resin was notably different from DDM and PPG400. The first heating cycle revealed two cure peaks in the profile at ~ 375 K and ~ 481 K while the second heating cycle had two T_g at ~ 350 K and ~ 380 K, Figure S2A. The two cure peaks and T_g suggest the formation of two distinct regions in the network of 3253 thermoset under the heating conditions used for the DSC analysis.

Differential scanning calorimetry analysis of the six cured thermoset samples showed all samples had an irreversible endothermic step around 323 K marked as polymer relaxation in Figure 2. This irreversible transition for both 3253 and DDM thermosets was broad while the transition for PPG400 was sharp. This transition is expected to be an artifact of the sample preparation as it

was not observed in the DSC analysis of the uncured samples, Figure S2. A polymer prepper tool from Frontier was utilized to prepare the samples in powder form. This is done by filing off polymer by hand which prevents chemical changes to the samples from heating, which is a concern in ball milling preparation. However, this irreversible transition seen at the same temperature for all samples indicates there is physical stress introduced into the polymer networks from the powder preparation process that is released at relatively low temperatures via enthalpy relaxation. The broad transition of this stress in 3253 and DDM thermosets is a consequence of being below the T_g for these thermosets while the sharp transition of this stress in PPG400 thermoset is a result of being above the T_g.

The PPG400 RT and PPG400 PC thermosets had identical T_g to the PPG400 uncured resin after curing in the second heating cycle. In addition, there is no evidence of residual cure in both the room temperature cured sample and the post cured sample confirming both treatments result in a 100% cured thermoset, Figure 2E/F and Table 2. Conversely, both DDM RT and DDM PC samples showed residual curing in the DSC profiles with calculated extent cures of 87% for DDM RT and 98% for DDM PC, Figure 2C/D and Table 2. The second heating cycle for both DDM RT and DDM PC had only the T_g transition which was identical to T_g the observed for the uncured sample, Figure S2B.

Differential scanning calorimetry of 3235 RT thermoset revealed both cure peaks in the first heating cycle at approximately 375 K and 410 K. The second cure peak is notably lower in temperature than the cure peak observed in the uncured 3253 resin by ~ 70 K, Figure S2A. In addition, the second heating cycle had only a single T_g at 375 K. These stark differences reveal that the structure of the final polymer network for the homopolymerized 3253 thermoset is highly influenced by heating parameters while the amine cured thermoset of DDM and PPG400 are not

likely resulting from differences in curing chemistry between the amine cured reaction and homopolymerization. Though both curing peaks are present in the first heating cycle of the 3253 RT thermoset, it is unclear how the second curing peak is related to curing peaks observed in uncured 3253 resin, therefore the calculated cure extent of 82% for the 3253 RT thermoset is labeled as an estimated cure extent, Table 2. Finally, after post cure the 3253 PC sample revealed no curing peaks in the first heating cycle confirming 100% cure, Figure 2B and Table 2. The T_g of 3253 PC matched the 3253 RT sample, Figure 2A/B.

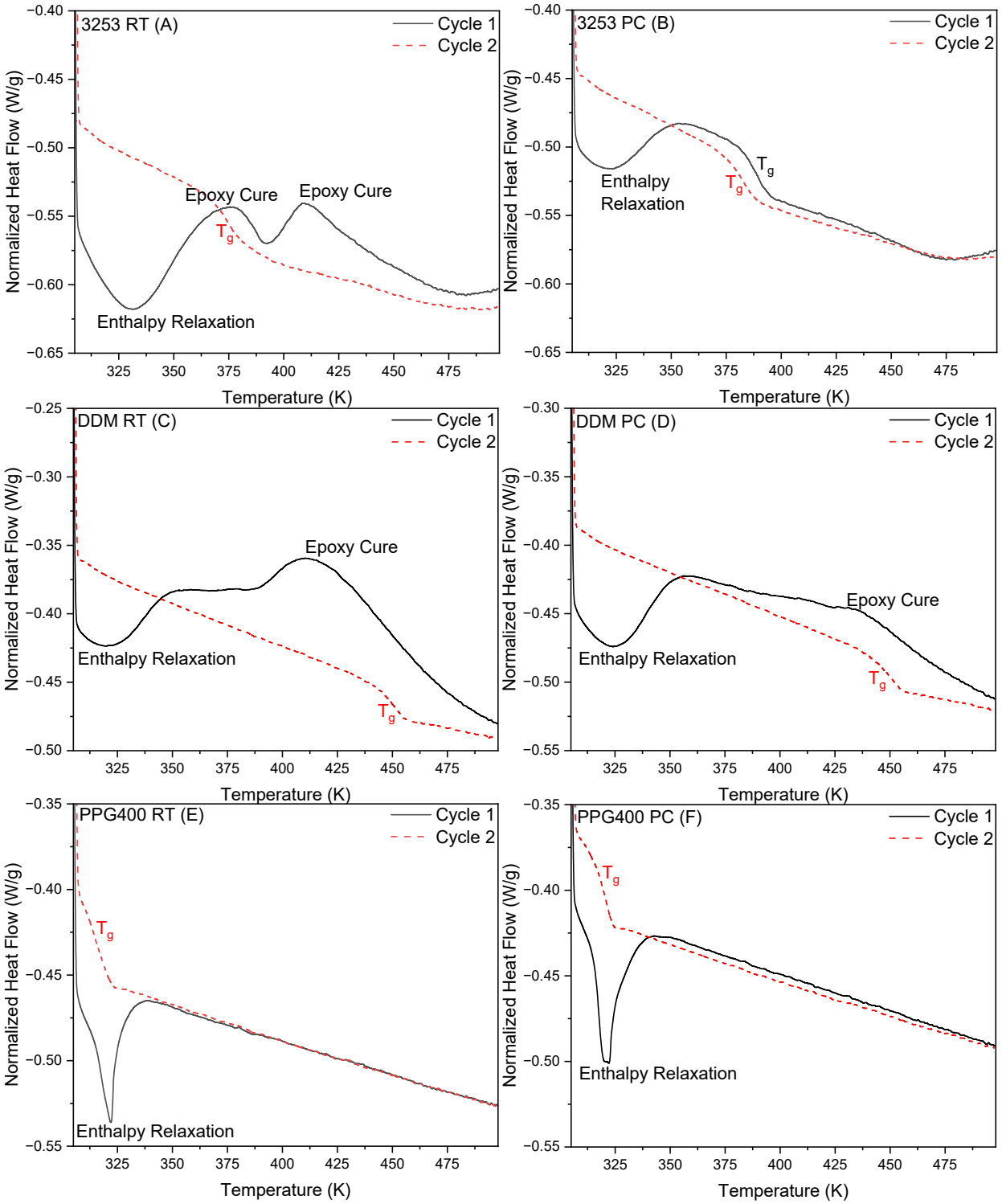

Figure 2. DSC results for 3253 RT (A), 3253 PC (B), DDM RT (C), DDM PC (D), PPG400 RT (E), and PPG400 PC (F) thermosets.

Table 2. Calculated cure extent for each thermoset formulation and cure conditions based on DSC data. The cure extent for 3253 RT is estimated (*) because it is unclear if the two cure peaks observed in the DSC cured 3253 are identical to the peaks observed in the 3253 RT sample due to their different positions in the DSC temperature profiles.

Sample	Cure Extent
3253 RT	*82%
3253 PC	100%
DDM RT	87%
DDM PC	98%
PPG400 RT	100%
PPG400 PC	100%

While no changes in the polymer chemistry are expected from the powder prepping process (because a manual polymer prepper was used) differences in the material properties of the polymer could causes differences in the size and morphology of the corresponding powders which could impact the degradation kinetics. To verify consistency of the size and morphology of the polymer powders between all samples, SEM images were taken (Figure 3). The SEM images show that all powdered samples have a shaven like morphology and particles are roughly 200 – 300 μm in size. This suggests that the material properties of the individual polymer types investigated are similar enough as to not impact the morphology or size of the particulates suggesting that observed differences in the kinetics between samples are not resultant from differences in particle morphology.

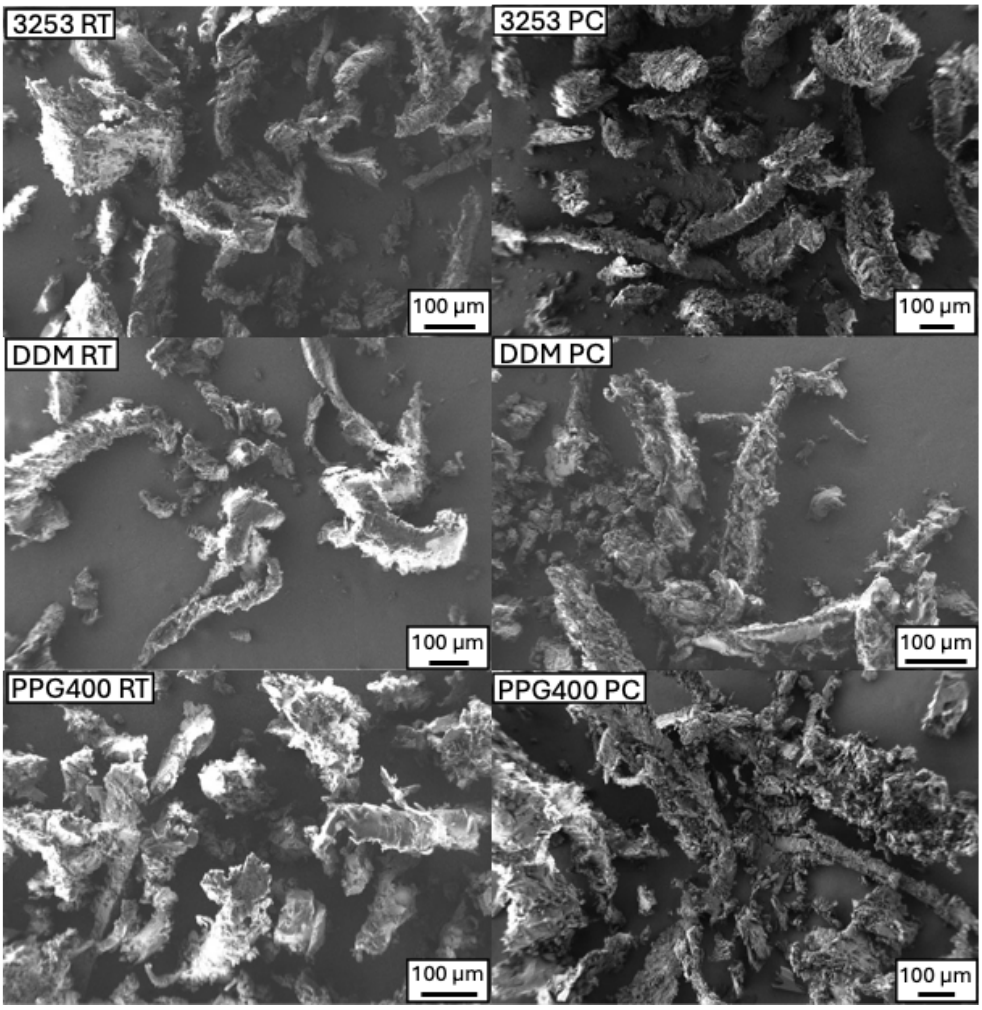

Figure 3. SEM images of 3253 RT, 3253 PC, DDM RT, DDM PC, PPG400 RT, and PPG400 PC showing consistent size and morphology of the polymer powders prepared with the prepping tool prior to EGA-MS analysis.

Wide angle X-ray scattering (WAXS) and low field ^{1}H nuclear magnetic resonance (NMR) was used to further interrogate the thermoset polymer network structures and provide further insight into the potential differences in BPA monomer packing environments. The WAXS pattern was measured in two ranges: 0.1–0.6 Q (Å)$^{-1}$ and 0.6–4.5 Q (Å)$^{-1}$, Figure 4. The major peak in Figure 4B has been identified previously as the π–π stacking of nearby aromatic rings in the network while the smaller peak in Figure 4A has been associated with the distance between hardener units

(H-H) in the network.[6] The H-H distances showed that the 3253 PC thermoset had the largest distance followed by DDM PC and PPG400 PC thermoset which had the shortest H-H distances.

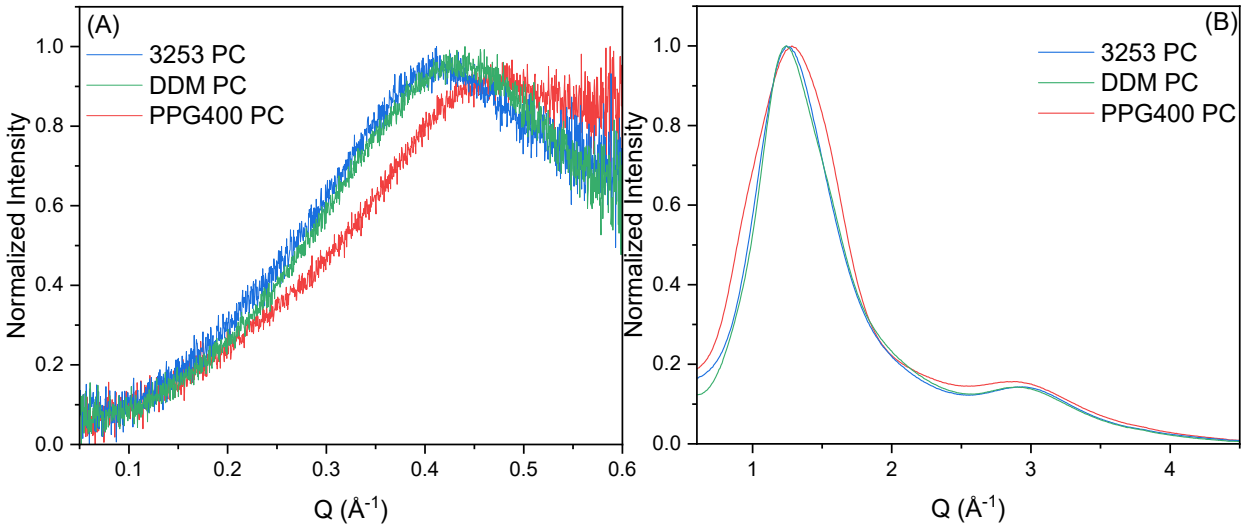

Figure 4. Wide angle X-ray scattering measurements for 3253 PC, DDM PC, and PPG400 PC thermosets showing (A) 0.1–0.6 Q (Å)$^{-1}$ range with the H-H peak and (B) 0.6–4.5 Q (Å)$^{-1}$ range with the aromatic π–π stacking peak.

The π–π stacking distances did not show a discernable trend between thermosets. Further, 3253 PC and DDM PC thermosets have very similar position and width of the peak attributed to π–π stacking. However, PPG400 PC thermoset has a notably broader π–π stacking peak which would suggest a greater diversity of π–π stacking distances, which could result from polydispersity of the PPG400 hardener. The polydispersity and flexibility of the PPG400 hardener likely causes different packing arrangement and conformations around the BPA monomer units. In contrast, the shorter, more rigid hardener units for 3253 and DDM thermosets would restrict the number of conformation available around the BPA monomer units causing a narrower π–π stacking peak.

Low field time domain ^{1}H NMR was used to measure the FID response of the protons present in the thermosets which provides more information about the local environment of the protons and in turn information of the polymer networks. Soft domains (Awb) represent domains where the

protons have greater mobility on the molecule with longer FID decay times while rigid domains (Ag) have less mobility and cause the FID to decay rapidly. Semi-rigid domains (Ag) represent domains in-between rigid and soft. The FID responses for Aa, Ag, and Awb are shown in Figure 5.

There was an increase in the FID Aa component, the most rigid proton fraction, from 3253 PC to PPG400 PC thermosets with 3253 PC having the lowest Aa component and PPG400 PC having the highest Aa component. The opposite trend was present for the Awb content, softest proton fraction, Figure 5. The greater rigid proton content in PPG400 can be explained by closer packing of the hardener components which contain the greatest proton content in the polymer structure. This is confirmed by WAXS results showing PPG400 thermoset has the shortest H-H distance. Based on these results it can be concluded that PPG400 has a flexible polymer network with a larger number of packing arrangements around the BPA monomer units. On the other hand, DDM thermoset is the most rigid while 3253 falls somewhere in between PPG400 and DDM.

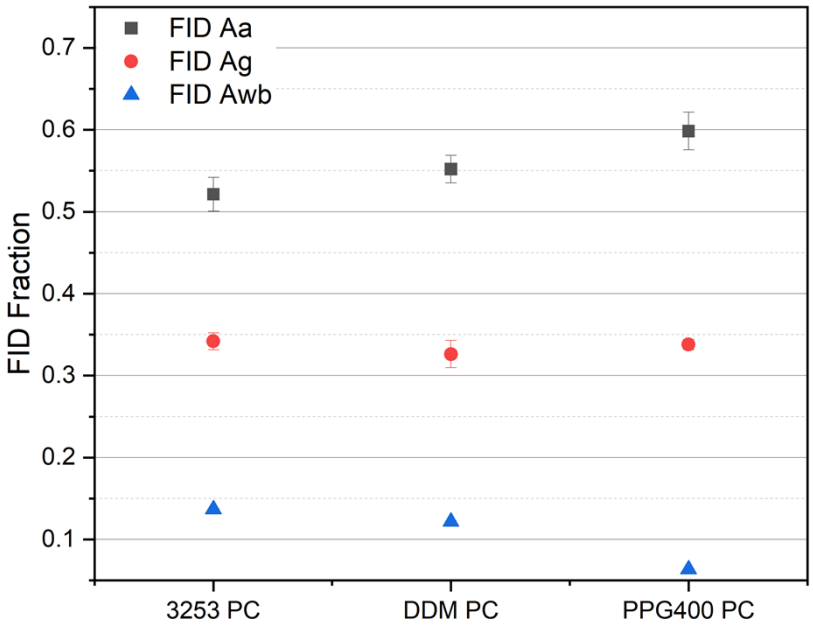

Figure 5. Proton NMR (^{1}H NMR) of FID phase fractions Aa, Ag, and Awb fit according to eq 4.

Pyrolysis-GC-MS was performed on each thermoset to validate that *m/z* 213 is a unique ion for BPA monomer formation. The resulting total ion chromatographs (TICs) and corresponding EICs are shown in Figure 6. The EICs reveal that in each formulation 79% or greater of the *m/z* 213 signal comes from BPA monomer, determined by integration of the total area under the *m/z* 213 peak. The remaining signal in each sample comes from instrument noise and other minor products. This confirms that the *m/z* 213 ion is unique for the BPA monomer and suitable for PSK analysis.

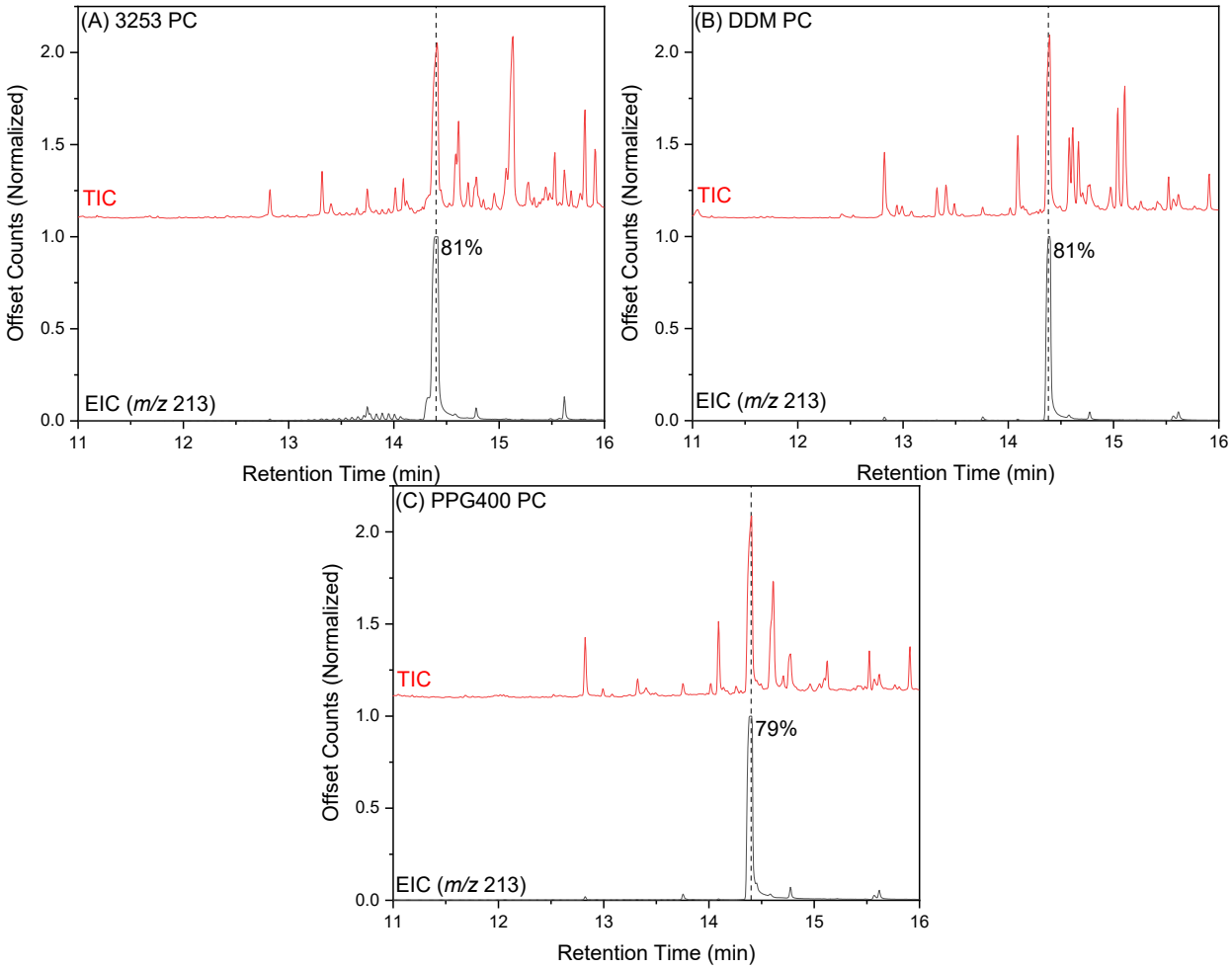

Figure 6. TICs with corresponding EICs of ion *m/z* 213, representing the unique ion of BPA monomer and showing the percent contribution of BPA monomer to the ion signal by peak area analysis for 3253 PC (A), DDM PC (B), and PPG400 PC (C).

The thermal profiles for both scanning mode and SIM mode were obtained at 2, 5, and 10 K/min heating rates for isoconversional analysis. Scanning mode mass spectrometry experiments monitor a large range of ions (*m/z* 29–500) and generates a Total Ion Thermograph (TIT) that represents the entirety of the sample with thermal profiles analogous to thermal gravimetric analysis.[27] Conversely, SIM mode monitors a single ion and produces a Single Ion Thermograph (SIT) of that ion. When the selected ion is unique for a specific product, the obtained SIT represents the formation of that product during the degradation and in turn that products' kinetics, making the analyte suitable for PSK analysis.[14]

The TIT and EIT thermal profiles for 3253 RT and 3253 PC thermosets are shown in Figure 7. The TITs of 3253 RT and 3253 PC show a primary pyrolysis peak with a shoulder emerging at low temperatures. After post curing this shoulder feature increases in intensity. The SIT of the *m/z* 213 ion reveals this same shoulder feature is present in 3253 RT and 3253 PC, Figure 7C/D. The increase in this shoulder peak is much more prominent in the SIT of 3253 PC sample than in the TIT. The presence of this shoulder feature in the SIT suggests that there are two regions in the polymer network with distinct thermal stabilities which would support the existence of different network configurations within the 3253 polymers. The presence of two different network configurations is hinted at in the DSC data with the presence of two T_g in the uncured DSC data. However, only one T_g was observed in the ex-situ cured 3253 RT and 3253 PC thermosets.

Because the DSC results show significant differences in the polymer networks between the in-situ DSC cured 3253 thermoset and the ex-situ cured samples an EGA-MS analysis was performed on the 3253 polymer recovered from the DSC cup. The TIT of the in-situ cured 3253 thermoset is significantly broadened compared to the ex-situ cured sample, Figure S3A. The non-isothermal curing parameters of the DSC result in the lower temperature shoulder peak observed in the ex-

situ cured samples to be the prominent peak in the TIT. The Extracted Ion Thermographs (EICs) for the *m/z* 213 ion show a similar change with the shoulder peak now being the primary pyrolysis peak, Figure S3B. These results show that, like the DSC, the EGA-MS is sensitive to changes in the polymer networks.

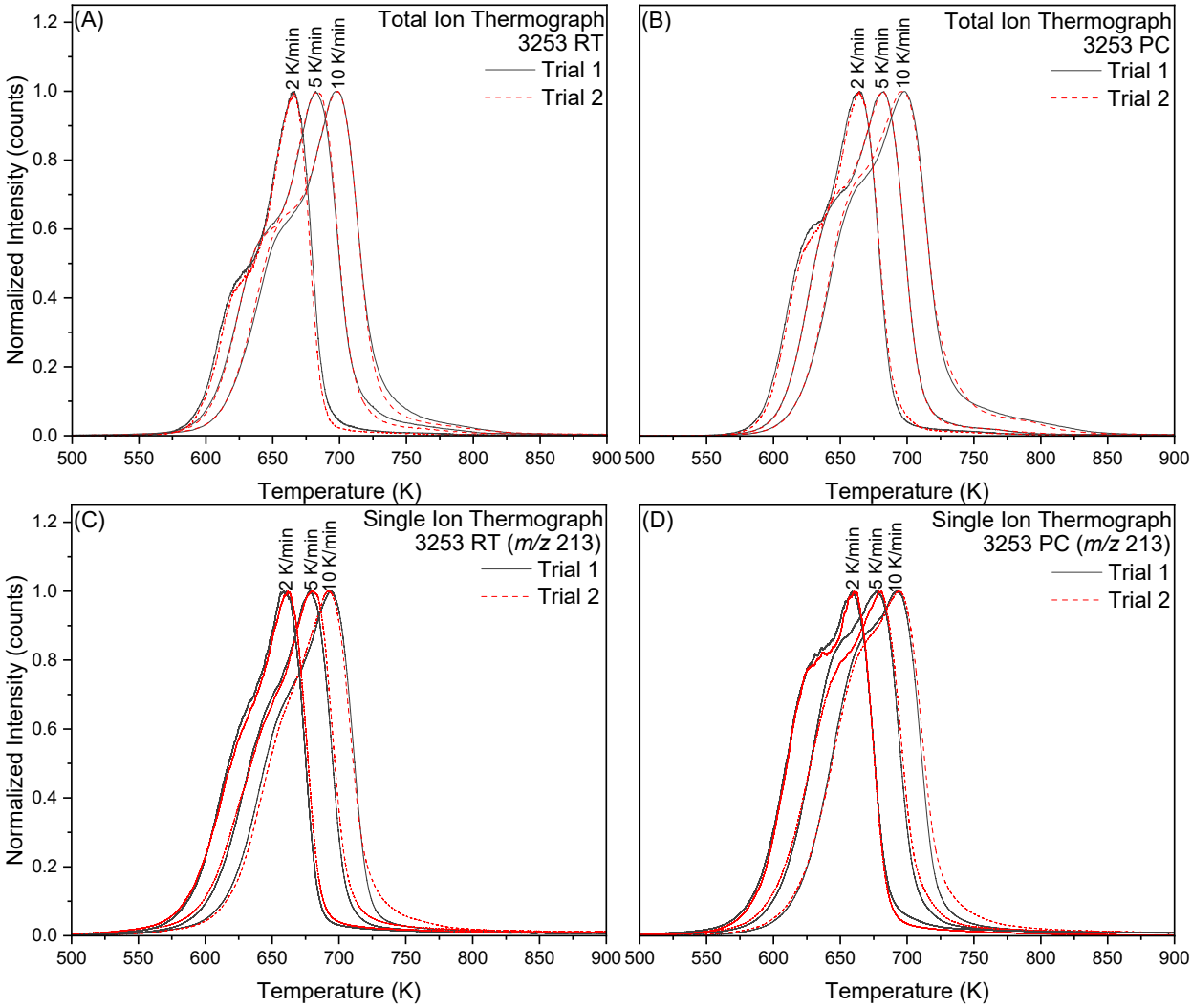

Figure 7. Normalized TITs of 3253 RT (A) and 3253 PC (B) with corresponding SIT of 3253 RT (C) and 3253 PC (D) showing a distinct shoulder feature on the primary peak in both the TITs and SITs.

Unlike the 3253 thermoset, DDM and PPG400 thermosets did not display a shoulder prior to the primary pyrolysis peak. Both DDM RT and DDM PC thermosets showed a single pyrolysis peak

in the TIT, Figure 8A/B. The SIT for DDM did not reveal any notable difference in the thermal profiles compared to the TIT profiles, Figure 8C/D. Similarly, the PPG400 thermosets have a single pyrolysis peak with a thermal profile that is consistent between the TIT and SIT, Figure 9. There is one notable difference in the SIT of PPG400. The SIT of both PPG400 RT and PPG400 PC appear to have a more sudden drop in the signal at the tail end of the pyrolysis peak, Figure 9C/D, compared to the DDM thermosets which have a gradual drop, Figure 8C/D.

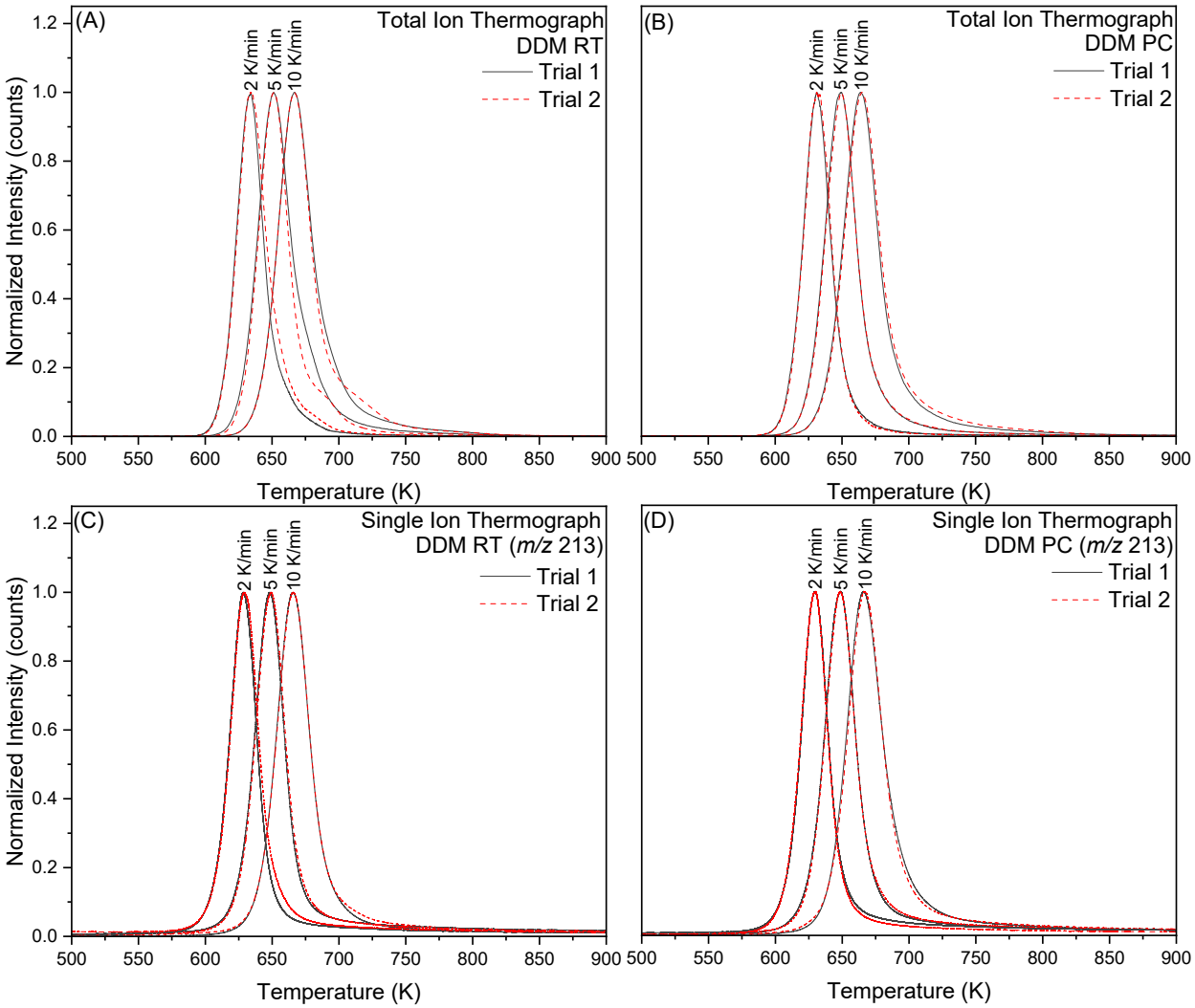

Figure 8. Normalized TITs of DDM RT (A) and DDM PC (B) with corresponding SIT of DDM RT (C) and DDM PC (D) showing a single primary pyrolysis peak in both the TITs and SITs.

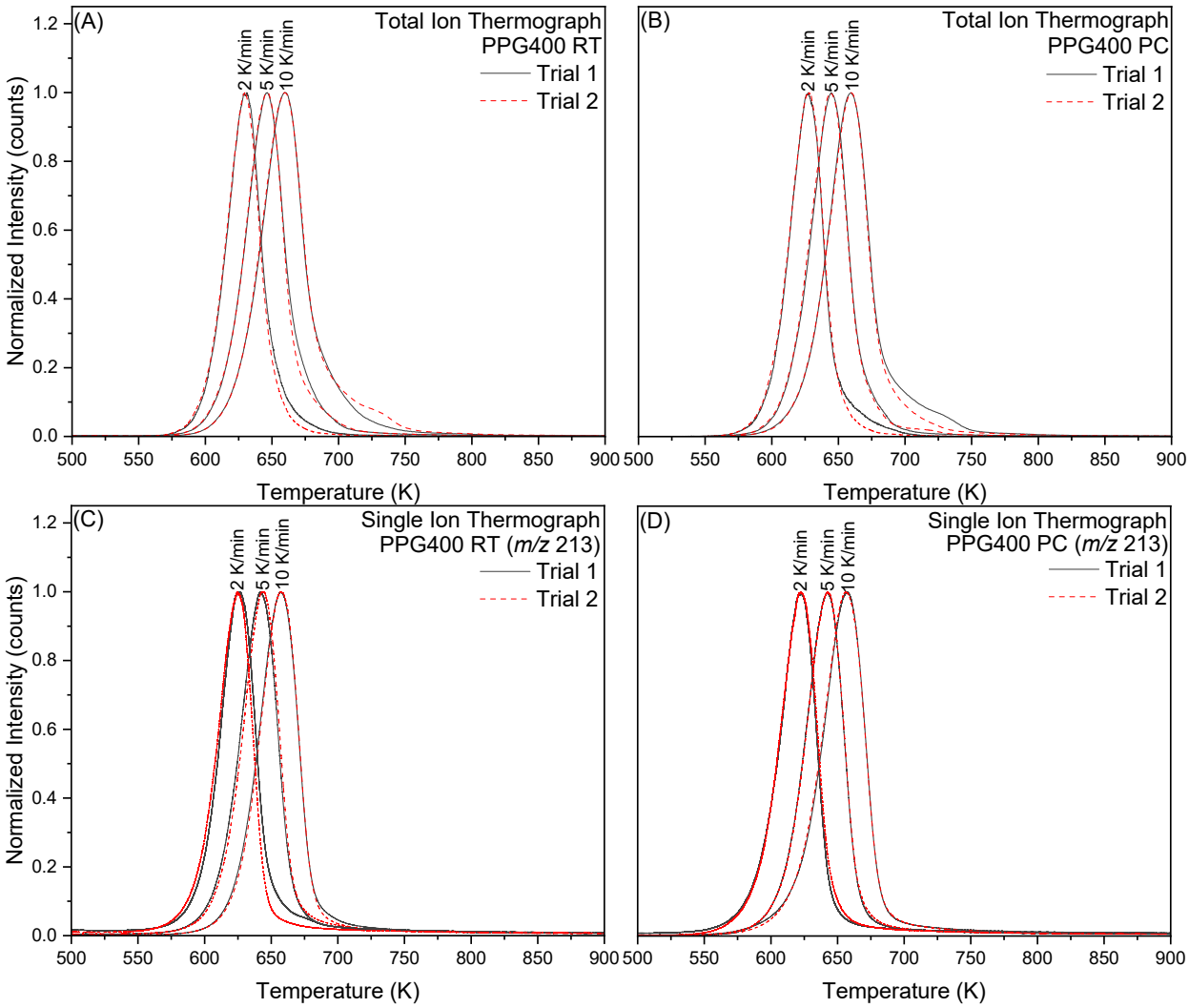

Figure 9. Normalized TITs of PPG400 RT (A) and PPG400 PC (B) with corresponding SIT of PPG400 RT (C) and PPG400 PC (D) showing a single primary pyrolysis peak in both the TITs and SITs.

Isoconversional kinetics and PSK analysis were used to determine the apparent E_a for both TITs and SITs. These results are shown in Figure 10 with corresponding extent conversion and kinetic plots presented in Figures S4-S9. The slope, y-intercept, and calculated error for the slope and y-intercept used for determining the apparent E_a at each conversion extent is in Table S2. Figure 10A shows the apparent E_a for the TIT thermal profiles of 3253 RT and 3253 PC. Thermoset 3253 RT has a gradual decrease in E_a over the course of the degradation starting at 210 kJ/mol and ending

at ~150 kJ/mol. Post curing has a notable impact on the overall apparent E_a of the thermoset lowering the apparent E_a from 0.1 – 0.6 α for 3253 PC compared to 3253 RT, Figure 10A.

Apparent E_a results from the SIT for the 3253 thermoset, Figure 10B, show significant differences in apparent E_a compared to the corresponding TIT results. The apparent E_a of the *m/z* 213 ion for 3253 RT thermoset shows a relatively consistant E_a over the course of the degradation peaking at 0.5 α. After post cure, the apparent E_a for 3253 PC is significantly lower from 0.2 – 0.6 α with the largest decrease occuring early in the degradation at 0.3 α, Figure 10B. This early part of the degradation corresponds to the shoulder peak in the SIT profiles, Figure 7D. When comparing the shoulder features of 3253 RT to 3253 PC, Figures 7C and 7D, the shoulder present in 3253 RT is not as prominent as the shoulder in 3253 PC, which is likely the reason it does not manifest as distincly in the apparent E_a results.

The trend in apparent E_a of the TIT thermal profiles for DDM (Figure 10C) and PPG400 (Figure 10E) are very similar to 3253 although the absolute scale is different due to differences in thermal stability of the polymers. The apparent E_a for TIT thermal profiles of both DDM and PPG400 show a gradual decrease in apparent E_a over the course of the degradation with the post cured versions of both thermosets favoring lower apparent E_a. The apparent E_a derived from the SIT, however, show very different trends between DDM and PPG400 thermosets. The results for DDM show, like the TIT results, a gradual decrease in apparent E_a over the course of the degradation with the DDM PC sample favoring lower apparent E_a, Figure 10D. Conversely, both PPG400 RT and PC thermosets showed a very consistent apparent E_a over the course of the degradation with PPG400 PC favoring lower apparent E_a, Figure 10F.

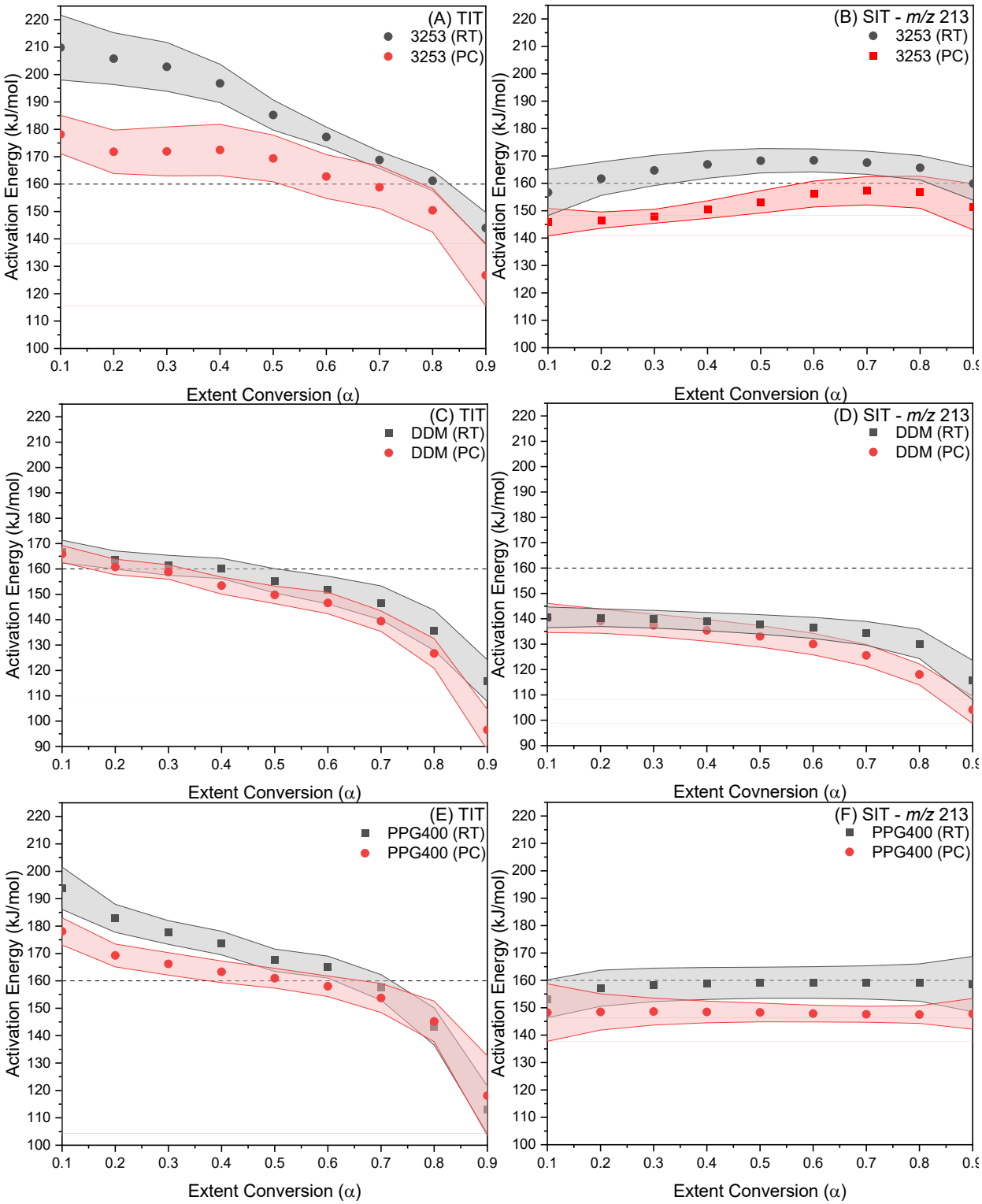
(A) TIT
3253 (RT)
3253 (PC)
(B) SIT - m/z 213
3253 (RT)
3253 (PC)
(C) TIT
DDM (RT)
DDM (PC)
(D) SIT - m/z 213
DDM (RT)
DDM (PC)
(E) TIT
PPG400 (RT)
PPG400 (PC)
(F) SIT - m/z 213
PPG400 (RT)
PPG400 (PC)
Activation Energy (kJ/mol)
Extent Conversion (α)
Extent Covnersion (α)

Figure 10. Apparent activation energies obtained from TIT and SIT experiments for 3253 TIT (A), 3253 SIM (B), DDM TIT (C), DDM (D), PPG400 TIT (E), PPG400 SIM (F) with plotted uncertainty bands shown. The E_a of 160 kJ/mol was marked for clarity of data interpretation.

The observed differences in apparent E_a from the SIT are hypothesized to be a consequence of different local packing densities around the BPA monomer units between the different thermoset formulations. In principle, in an ideal system, there should be no reasons for identical BPA monomer formations to have different apparent activation energies. Thus, differences in local packing density are theorized to potentially impact the observed kinetics in one of two ways: (1) more time is required for the freed BPA monomer to escape higher local packing density compared to lower density packing regions causing it to be detected at higher temperatures after the host structure has undergone greater thermal distortion or (2) the higher local packing density regions prevent the formed radical monomers from rapidly escaping the reaction site allowing for a greater equilibrium constant between the free radical and bound monomer state compared to the lower density regions, Figure 11.

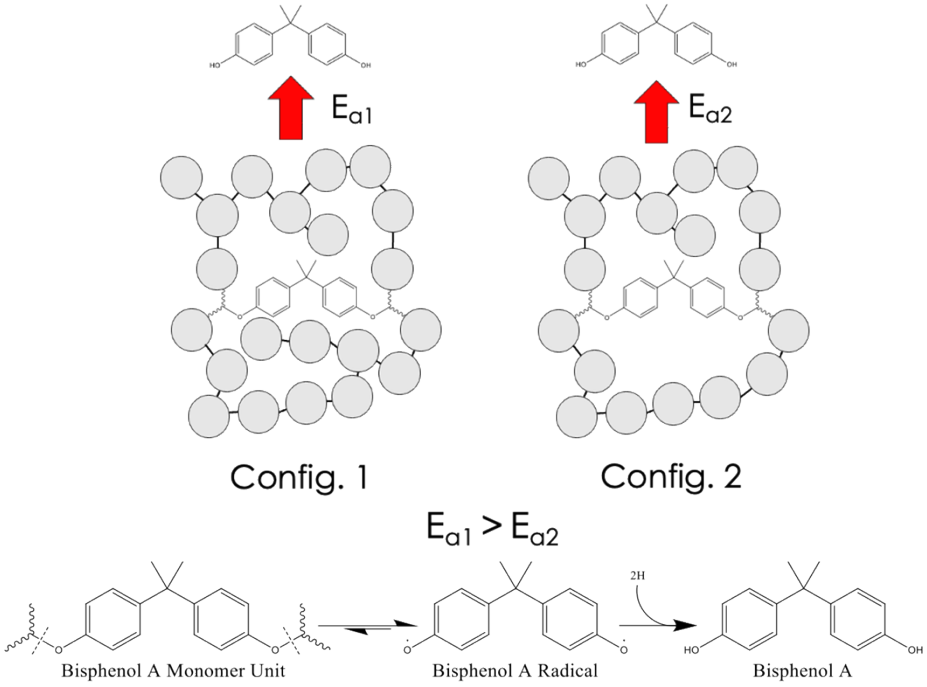

Figure 11. Scheme of proposed polymer packing differences causing differences in E_a for identical BPA formation mechanisms along with BPA formation mechanisms from pyrolysis.

Thus, we demonstrate that the differences observed in the apparent E_a for the SIT of all samples can be explained by differences and/or changes in local packing densities around the BPA monomer units. This is consistent with the fact that in each sample, post curing was observed to decrease the overall apparent E_a, even in the case of PPG400 thermoset where no additional curing occurs. In a previous study the impact of 423 K thermal exposure on the network structures of similar polymer thermosets was investigated with WAXS.[6] After a one hour exposure at 423K, an increase in the aromatic π-π stacking distances was observed and attributed to polymer network rearrangement. The increase in π-π stacking distances would suggest that the local network arrangement around the BPA monomer units become more open (i.e. less dense). A similar effect can be expected for the thermosets investigated in this study. The hypothesized decrease in local packing density around the BPA monomer units would manifest as a decrease in the apparent E_a which is what is observed after post curing in all samples.

The differences in apparent E_a trends between thermosets from the SIT is best observed in Figure 12 which shows 3253 PC, DDM PC, and PPG400 PC normalized to their respective E_a at 0.1 α for comparison. Figure 12 shows significant differences in apparent E_a between each thermoset. 3253 PC thermoset has two distinct regions with 0.1-0.4 extent conversion having lower E_a and 0.5-0.9 having significantly higher E_a. The significant difference in these regions for 3253 PC suggests the existence of two distinct packing densities within the 3253 thermosets, which is further supported by the data in the SIT showing a distinct shoulder peak. The existence of two regions in the 3253 polymer network is also supported by the DSC results for the in-situ cured thermosets.

Consequently, the results are consistent with a lower determined E_a signifying a lower packing density while the higher E_a signifies higher packing density. The formation of the lower packing density arrangment in 3253 is postulated to be a secondary packing structure that forms at the later stages of cure when polymer mobility is restricted. At the early stages of cure, prior to significant crosslinking, the polymer chains will have mobility to arrange in a more desirable higher packing efficiency (i.e. density) arrangment. But after significant crosslinking occurs, the mobility of the polymer decreases significantly resulting in the formation of a less densely packed arrangment, and supported by the increase of the shoulder peak in the SIT after post cure which indicates the increasing concentration of these structures in the polymer network. The observation that the lower density packing structure gives rise to the primary peak in the TIT after a non-isothermal cure in the DSC is also supported by this scenario as the more rapid curing conditions would hinder denser packing of the polymer network. Interestingly, the fact that these two packing densities are observed in the EGA-MS both qualitatively from changes in SIT peak shape and quantitatively via changes in the E_a in the EGA-MS results but are not consistently observed in the DSC suggest

these structures are not directly linked to the T_g of the polymer. Therefore, EGA-MS can be more sensitive to certain network structures of amorphous thermosets that DSC and other structural characterization techniques cannot observe and is a highly complimentary characterization technique for amorphous polymer networks of thermosets.

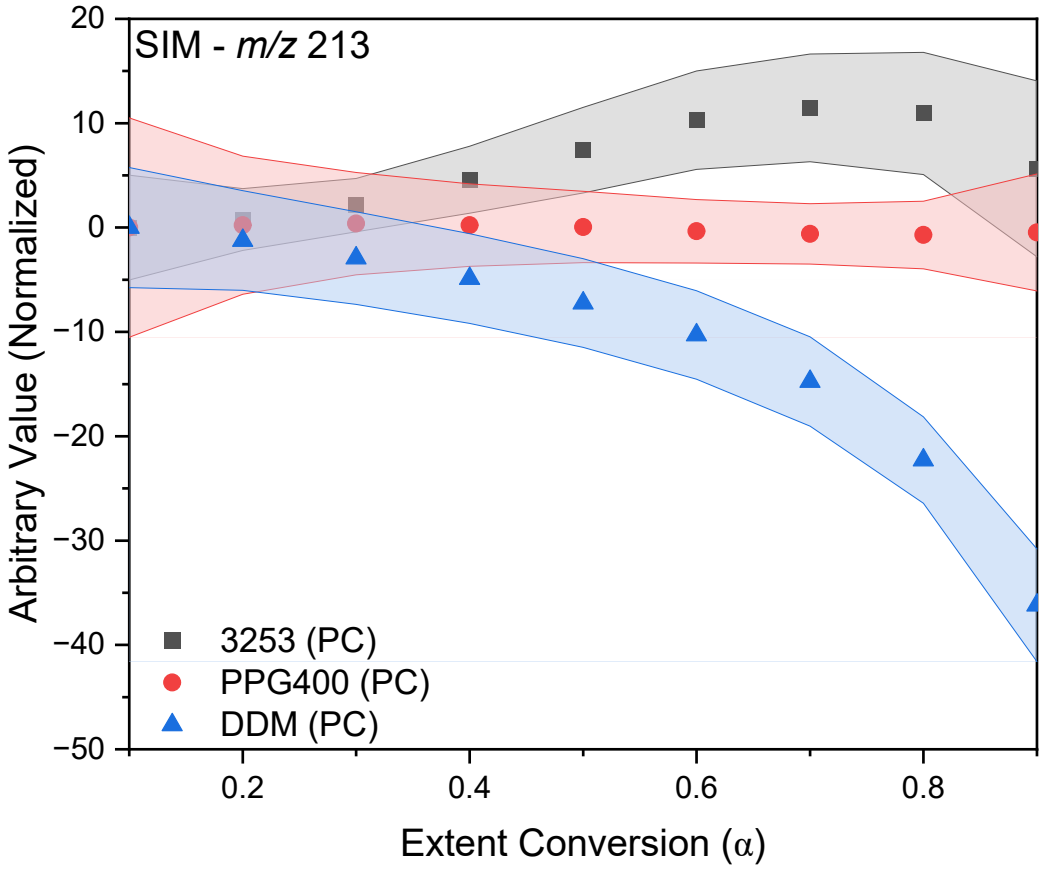

Figure 12. Apparent E_a of the SIT for 3253 PC, DDM PC, and PPG400 PC samples normalized to their respective 0.1 α values for comparison showing each thermoset has distinct apparent E_a profiles, hypothesized to result from differences in polymer packing density.

Continuing to discuss Figure 12, the apparent E_a for both DDM PC and PPG400 PC thermosets are significantly different from 3253 PC. PPG400 PC has a relatively consistent E_a over the course of the degradation and DDM shows gradually decreasing as a function of extent conversion E_a. The lack of distinctive shoulders in the DDM PC and PPG400 PC (Figures 8D and 9D) SIT profiles

suggest both networks have regular packing arrangements throughout the polymer network. the change in apparent E_a is notably different. The biggest difference between DDM and PPG400 networks is the T_g with DDM having the highest T_g and PPG400 having the lowest. The higher T_g of DDM is supportive of DDM having a much more rigid polymer network due to the high number of aromatic functional groups present from both the epoxy and hardener. Conversely, PPG400 would have the most flexible matrix due to the longer linear chain of the hardener which would allow significantly more mobility than in the case of the DDM thermoset. Therefore, during degradation the higher mobility of PPG400 would allow for rearrangements of the network during BPA monomer release resulting in a relatively consistent packing density around the remaining BPA monomer units and, in turn, a consistent E_a.

On the other hand, the rigid nature of the DDM thermoset would prevent significant rearrangement of the network after BPA monomer release leaving a void in the nearest neighbor BPA monomer unit. The presence of this void would subsequently decrease the local packing density of that monomer and, consequently, lower the E_a required for release. This process would be compounded over the course of the degradation and manifest as a decreasing apparent E_a at higher conversion extents. The lack of the gradual decrease in 3253 thermoset suggests that there is sufficient polymer mobility during degradation to compensate for this effect like PPG400 thermoset. It is important to note that while there is improved polymer mobility above T_g for thermosetting materials the crosslinking arrangements in the polymer are maintained. Therefore, while 3253 PC thermoset has improved polymer mobility during degradation the fixed crosslinking network locks in the two distinct packing densities which is why two distinct regions are observed.

Conclusion

We demonstrate the use of EGA-MS to interrogate the polymer network packing arrangements in BPA-based polymer thermosets. It was hypothesized that the shape of the thermal profile for a unique ion of BPA monomer formation (*m/z* 213) is indicative of the local packing density around the BPA monomer units in the polymer network. This was thought to manifest qualitatively as changes in peak shape of the *m/z* 213 profile and quantitatively as changes in the apparent activation energy (E_a) of the BPA monomer formation.

Results revealed two distinct packing densities exist in 3253 thermosets while DDM and PPG400 thermosets have uniform distributions of packing densities. DDM had a gradual decrease in apparent E_a which was postulated to be due to decreasing packing density around the nearest neighbor BPA monomer units as BPA monomers are released during degradation. Conversely, PPG400 thermoset had a consistent E_a over the course of the degradation. The difference in E_a response between PPG400 and DDM thermoset is hypothesized to result from the polymer mobility during degradation with PPG400 having a much more flexible and mobile matrix which allows for rearrangements to occur around the BPA monomers providing a consistent packing density. DDM thermoset, on the other hand, has a much more rigid matrix which prevents rearrangement causing a continuously decreasing local packing density around the BPA monomer units consequently causing a gradual decrease in E_a. Interestingly, the EGA-MS technique appears to be particularly sensitive to these differences in network structures. The differences in packing density appear as both qualitative changes in the SIT profile shape and quantitative changes in the E_a and these density changes were not detected with DSC measurements. This suggests that these packing arrangements are not directly linked to the T_g of the polymer network or, at least, manifest as a minute change that was not detectable with the DSC instrumentation used. These results

present insight into the nature of thermoset polymer network packing arrangements; their behavior during thermal degradation; and demonstrate an alternative technique that can be used to interrogate polymer networks structures of thermosetting materials that are not readily detectable by other techniques. Because this is a minimally destructive technique it would be particularly advantageous for characterization of composite parts to evaluate changes in the network structures from prolonged use. It is important to note that while this methodology is suitable for any crosslinked thermosetting polymer with unique ions for the monomer units it is not suitable for thermoplastic polymers which would undergo a melting transition prior to degradation which would erase any network packing features.

Supporting Information

DSC data, End Point Weighted Correction values, Conversion plots, kinetics plots, and table with numerical values extracted from kinetic plots

Acknowledgments

This work was sponsored by the National Nuclear Security Administration.

References

(1) Jin, F. L.; Li, X.; Park, S. J. Synthesis and application of epoxy resins: A review. *J. Ind. Eng. Chem.* **2015**, *29*, 1-11. DOI: 10.1016/j.jiec.2015.03.026.
(2) Knox, S. T.; Wright, A.; Cameron, C.; Fairclough, J. P. A. Well-Defined Networks from DGEBF-The Importance of Regioisomerism in Epoxy Resin Networks. *Macromol.* **2019**, *52* (18), 6861-6867, Article. DOI: 10.1021/acs.macromol.9b01441.
(3) Knox, S. T.; Wright, A.; Cameron, C.; Fairclough, J. P. A. Structural Variation and Chemical Performance-A Study of the Effects of Chemical Structure upon Epoxy Network Chemical Performance. *ACS Appl. Polym. Mater.* **2021**, *3* (7), 3438-3445. DOI: 10.1021/acsapm.1c00378.
(4) Challis, R. E.; Freemantle, R. J.; Fuller, W.; Martin, C. M.; Mahendrasingham, A.; Chadwick, D.; Cocker, R. P. *Epoxy Cure Observed by Ultrasound, NMR and WAXS. In Thompson, D.O., Chimenti, D.E. (eds) Review of Progress in Quantitative Nondestructive Evaluation. Review of Progress in Quantitative Nondestructive Evaluation*; 1999, *18*, 2185-2189. DOI: https://doi.org/10.1007/978-1-4615-4791-4_280.
(5) Lovell, R.; Windle, A. H. WAXS INVESTIGATION OF LOCAL-STRUCTURE IN EPOXY NETWORKS. *Polym.* **1990**, *31* (4), 593-601. DOI: 10.1016/0032-3861(90)90274-3.
(6) Dwyer, D. B.; Isbill, S. B.; Brubaker, Z. E.; Keum, J. K.; Bras, W.; Niedziela, J. L. Thermally Induced Structural Transitions in Epoxy Thermoset Polymer Networks and Their Spectroscopic Responses. *ACS Appl. Polym. Mater.* **2023**, *5*, 5961-5971.

(7) Matyi, R. J.; Uhlmann, D. R.; Koutsky, J. A. STRUCTURE OF GLASSY-POLYMERS .7. SMALL-ANGLE X-RAY-SCATTERING FROM EPOXY-RESINS. *J. of Polym. Sci, Part B: Poly. Phys.* **1980**, *18* (5), 1053-1063. DOI: 10.1002/pol.1980.180180512.
(8) Ishida, T.; Kitagaki, R.; Elakneswaran, Y.; Mizukado, J.; Shinzawa, H.; Sato, H.; Hagihara, H.; Watanabe, R. Network Degradation Assessed by Evolved Gas Analysis-Mass Spectrometry Combined with Principal Component Analysis (EGA-MS-PCA): A Case of Thermo-Oxidized Epoxy/Amine Network. *Macromol.* **2023**, *56* (3), 883-891. DOI: 10.1021/acs.macromol.2c02383.
(9) Watanabe, R.; Nakamura, S.; Sugahara, A.; Kishi, M.; Sato, H.; Hagihara, H.; Shinzawa, H. Revealing Molecular-Scale Structural Changes in Polymer Nanocomposites during Thermo-Oxidative Degradation Using Evolved Gas Analysis with High-Resolution Time-of-Flight Mass Spectrometry Combined with Principal Component Analysis and Kendrick Mass Defect Analysis. *Anal. Chem.* **2024**, *96* (6), 2628-2636. DOI: 10.1021/acs.analchem.3c05269.
(10) Gong, X. Y.; Liu, Y. Y.; Wu, S. Q.; Ding, D. W.; Wei, H. G.; Guo, Z. H. Decomposition mechanisms of cured epoxy resins in near-critical water. *J. Appl. Polym. Sci.* **2015**, *132* (11). DOI: 10.1002/app.41648.
(11) Evangelopoulos, P.; Kantarelis, E.; Yang, W. H. Investigation of the thermal decomposition of printed circuit boards (PCBs) via thermogravimetric analysis (TGA) and analytical pyrolysis (Py-GC/MS). *J. Anal. Appl. Pyrolysis* **2015**, *115*, 337-343. DOI: 10.1016/j.jaap.2015.08.012.
(12) Zeng, Y. K.; Xue, Y.; Gong, X.; Gao, X.; E, J. Q.; Chen, J. W.; Leng, E. W. Pyrolytic performance and kinetics study of epoxy resin in carbon fiber reinforced composites: Synergistic effects of epoxy resin and carbon fiber. *J. Anal. Appl. Pyrolysis* **2023**, *176*, 106255. DOI: 10.1016/j.jaap.2023.106255.
(13) Dwyer, D. B.; Isbill, S. B.; Niedziela, J. L.; Kapsimalis, R. J.; Duckworth, D. C. Influence of temperature on accessible pyrolysis pathways of homopolymerized bisphenol A/F epoxies and copolymers. *J. Anal. Appl. Pyrolysis* **2021**, *153*, 104978. DOI: 10.1016/j.jaap.2020.104978.
(14) Dwyer, D. B.; Gallego, N. C.; Isbill, S.; Miskowiec, A.; Niedziela, J. L. Product-specific kinetics reveal effect of epoxy crystallization on thermoset thermal degradation. *Polym.* **2024**, *301*, 127003.
(15) Dwyer, D. B.; Gallego, N. C.; Niedziela, J. L.; Kapsimalis, R. J.; Duckworth, D. C. Product Specific Thermal Degradation Kinetics of Bisphenol F Epoxy in Inert and Oxidative Atmospheres using Evolved Gas Analysis-Mass Spectrometry. *J. Anal. Appl. Pyrolysis* **2022**, *165*, 105563. DOI: doi.org/10.1016/j.jaap.2022.105563.
(16) *Characterization of the Degree of Cure of thermosetting Resins by DSC*; TA389; https://www.tainstruments.com/pdf/literature/TA389.pdf, Accessed 11/10/25.
(17) Kim, Y. M.; Han, T. U.; Hwang, B.; Lee, Y.; Watanabe, A.; Teramae, N.; Kim, S. S.; Park, Y. K.; Kim, S. New approach for the kinetic analysis of cellulose using EGA-MS. *Polym. Test.* **2017**, *60*, 12-17, Article. DOI: 10.1016/j.polymertesting.2017.02.004.
(18) Vyazovkin, S. *Isoconversional Kinetics of Thermally Stimulated Processes*; Springer, 2015. DOI: 10.1007/978-3-319-14175-6.
(19) Akahira, T.; Sunose, T. Method of determining activation deterioration constant of electrical insulating materials. *Res. Report Chiba. Inst. Technol. (Sci Technol)* **1971**, *16*, 22-31.
(20) Starink, M. J. The determination of activation energy from linear heating rate experiments: a comparison of the accuracy of isoconversion methods. *Thermochim. Acta* **2003**, *404* (1-2), 163-176, Article. DOI: 10.1016/s0040-6031(03)00144-8.
(21) Maus, A.; Hertlein, C.; Saalwächter, K. A robust proton NMR method to investigate hard/soft ratios, crystallinity, and component mobility in polymers. Macromol. *Chem. Phys.* **2006**, *207*, 1150-1158.
(22) Saalwachter, K.; Soman, B.; Evans, C. M. Crystallinity and perfection in ethylene vitrimers probed by combined calorimetry, scattering, and time-domain NMR. *Front. Soft Matt.* **2023**, *3*, 1-11. DOI: https://doi.org/10.3389/frsfm.2023.1208777.
(23) Räntzsch, V.; Haas, M.; Özen, M.; Ratzsch, K.; Riazi, K.; Kauffmann-Weiss, S.; Palacios, J.; Müller, A.; Vittorias, I.; Guthausen, G.; Wilhelm, M., Polymer crystallinity and crystallization kinetics via benchtop ^{1}H

NMR relaxometry: Revisited method, data analysis, and experiments on common polymers. *Polym.* **2018**, *145*, 162-173. DOI: 10.1016/j.polymer.2018.04.066.
(24) Abragam, A. *Principles of Nuclear Magnetism*; Oxford University Press, 1983.
(25) Schäler, K.; Roos, M.; Micke, P.; Golitsyn, Y.; Seidlitz, A.; Thurn-Albrecht, T.; Schneider, H.; Hempel, G.; Saalwächter, K. Basic principles of static proton low-resolution spin diffusion NMR in nanophase-separated materials with mobility contrast. *Solid State Nucl. Magn. Reson.* **2015**, *72*, 50-63. DOI: 10.1016/j.ssnmr.2015.09.001.
(26) Alam, T.; Allers, J.; Jones, B. Heterogeneous Polymer Dynamics Explored Using Static 1H NMR Spectra. *Intern. J. Mol. Sci.* **2020**, *21* (15). DOI: 10.3390/ijms21155176.
(27) Shiono, A.; Hosaka, A.; Watanabe, C.; Teramae, N.; Nemoto, N.; Ohtani, H. Thermoanalytical characterization of polymers: A comparative study between thermogravimetry and evolved gas analysis using a temperature-programmable pyrolyzer. *Polym. Test.* **2015**, *42*, 54-61.

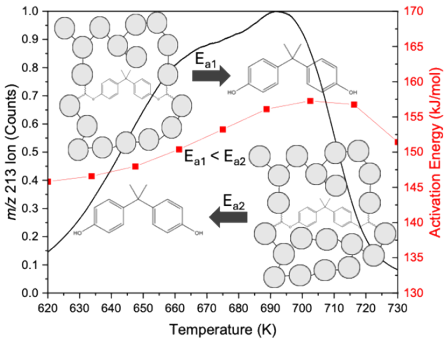

Table of Content Graphic